Two-Dimensional Symmetrical Mixtures in an External Field of Square Symmetry

A. Patrykiejew* and S. Sokołowski

Department for the Modelling of Physico-Chemical Processes, Faculty of Chemistry, MCS University, 20031 Lublin, Poland

Received: September 9, 2009; Revised Manuscript Received: October 26, 2009

Using the Monte Carlo simulation method in the grand canonical ensemble, we study two-dimensional symmetrical binary mixtures subjected to an external potential of square symmetry and finite corrugation. The results reveal a rich variety of mixed liquid-like and solid-like structures. It is demonstrated that even very weakly corrugated external potential leads to the development of axially ordered striped solid-like phases. The results of finite temperature simulation confirm quite well the predictions stemming from the ground state considerations and show the formation of commensurate, high-order commensurate, and incommensurate mixed phases. It is also shown that the corrugation potential affects the demixing transition.

I. Introduction

The phase behavior of one-component two-dimensional Lennard-Jones fluid has been intensively studied,[1−10] and the phase diagram of this system is rather well established. The system exhibits two-dimensional gas, liquid, and solid phases. The triple point and critical point temperatures have been estimated as being equal to $T_t^* = 0.400 \pm 0.01$ and $T_c^* = 0.51 \pm 0.02$, respectively. The only major controversy involves the nature of the melting transition,[5,6,11] though it is now widely accepted that two-dimensional solids melt via two continuous phase transitions, as predicted by the Kosterlitz−Thouless−Nelson−Haperin−Young dislocation-mediated melting theory.[12−16]

Also, phase transitions and ordering phenomena in two-dimensional one-component fluids subjected to an external corrugation potential are now rather well understood.[17−23] One should note that such systems are experimentally accessible, since adsorbed monolayers formed at low temperatures on crystals are effectively two-dimensional.[18,19,22]

Both experiments as well as computer simulations have demonstrated[21−23] that such films can form different commensurate, high-order commensurate, and incommensurate phases, depending both on the properties of the fluid and the substrate, and on the thermodynamic conditions (e.g., the temperature and the film density).

Our understanding of two-dimensional binary mixtures is much less advanced. The parameter space of such systems is very large and involves competing lengths and energies. As a result, the phase behavior of binary mixtures is much more complex than observed in one-component systems.[24,25] In order to gain some basic knowledge about the phase behavior of mixtures, a simple model of a symmetrical mixture was often used.[25−38] A symmetrical binary mixture is characterized by the same interactions between the pairs of like particles, while the interaction between a pair of unlike particles is different. The interest in such systems is also justified by the fact that a symmetrical mixture is a simple and yet quite reasonable model for racemic mixtures.[39−41]

The phase behavior of uniform three- and two-dimensional binary symmetrical mixtures has been the subject of quite intensive studies, though a vast majority of papers have dealt with fluid phases only and concentrated on the understanding of demixing transition and spinodal decomposition.[42−45] The formation of solid phases has been discussed in a few papers only.[40,46−48] Vlot and van der Eerden[46] have considered symmetrical Lennard-Jones mixtures characterized by different ratios of the Lennard-Jones potential parameters σ_{AB}/σ_{AA} ($\sigma_{BB} = \sigma_{AA}$), while keeping $\varepsilon_{AA} = \varepsilon_{BB} = \varepsilon_{AB}$. Using the Monte Carlo method in the isothermal−isobaric ensemble, they have observed the formation of liquids and solids of different structure depending on the magnitude of the ratio σ_{AB}/σ_{AA} and the temperature.

In our earlier work[49] (hereafter referred to as part I), we have discussed the ground state properties of two-dimensional symmetrical mixtures of Lennard-Jones particles subjected to an external periodic potential of square symmetry. It was shown that the corrugation potential leads to the formation of a variety of solid-like mixed phases of different structure, which depends on the properties of the mixture and on the height of the potential barrier between adjacent potential wells. Several commensurate phases of different densities were considered, including the axially ordered high-order $(3 \times 2)_{AB}$ commensurate phase and incommensurate phases. It was also demonstrated that the increase of the surface potential corrugation may reduce the stability of mixed phases, leading to phase separation which results in the formation of solid phases of pure components.

The main objective of the present work is to discuss the effects of external potential on the behavior of two-dimensional symmetrical mixtures and to verify the predictions stemming from the ground state calculations.[49] The parameter space of the model is much too rich to attempt a systematic study. Note that there are three relevant lengths, the size of lattice generated by the external potential (characterized by the lattice constant a) and the Lennard-Jones potential parameters, $\sigma_{AA} = \sigma_{BB}$ and σ_{AB}. Of course, $\sigma_{AA} = \sigma_{BB}$ in the case of symmetrical mixtures. Also, there are three energy-like parameters, the corrugation of the external field and the Lennard-Jones potential parameters: $\varepsilon_{AA} = \varepsilon_{BB}$ and ε_{AB}.

In the case of external potentials of finite corrugation, the parameters a, σ_{AA}, σ_{BB} ($=\sigma_{AA}$), and σ_{AB} determine the types of possible epitaxial structures in the system, and the following

* To whom correspondence should be addressed. E-mail: andrzej@pluto.umcs.lublin.pl.

10.1021/jp908710e
Published on Web 12/17/2009

situations can be met. (i) All neighbor pairs are allowed. (ii) Only the pairs of like atoms (A−A and B−B) can occupy adjacent sites, while the occupation of adjacent sites by A−B pairs is not possible. (iii) Only the pairs of unlike atoms can occupy adjacent sites, while it is not possible for the pairs of like atoms. (iv) Occupation of adjacent sites is not possible at all. Of course, one can also consider still larger atoms excluding the occupation of the first as well as second nearest neighbor sites.

In any of the above specified situations, the actual structure of condensed phases depends on the chosen values of the parameters a, σ_{AA}, σ_{AB}, ε_{AA}, and ε_{AB}, the height of the potential barrier between adjacent sites, as well as he temperature and density. In this paper, we confine the discussion to a series of systems with the fixed values of $\sigma_{AA}/a = 1.0$, $\sigma_{AB}/a = 1.24$, and $\varepsilon_{AB}/\varepsilon_{AA} = 1.0$. This choice of σ_{AA}/a and σ_{AB}/a corresponds to the above specified case (ii). Thus, we shall consider the situation in which the only parameter allowed to vary is the height of the potential barrier between adjacent sites.

The paper is organized as follows. In the section II, we describe the model and methods used. Section III presents the results. In part A, we discuss the behavior of the uniform system (with the external potential switched off), while, in part B, we consider the effects of periodic external potential on the properties of the system. Section IV gives a short summary and points out directions of future work.

II. The Model and Monte Carlo Methods

As already mentioned in the Introduction, we consider a two-dimensional symmetrical mixture consisting of atoms A and B, which interact via the truncated (12,6) Lennard-Jones potential

$$u_{ij}(r) = \begin{cases} 4\varepsilon_{ij}[(\sigma_{ij}/r)^{12} - (\sigma_{ij}/r)^{6}] & r \le r_{max} \\ 0 & r > r_{max} \end{cases} \quad (1)$$

where r is the distance between a pair of atoms and i and j mark the species A and B. In a symmetrical mixture, $\sigma_{AA} = \sigma_{BB} = \sigma$ and $\varepsilon_{AA} = \varepsilon_{BB} = \varepsilon$. The corresponding potential parameters for a pair of unlike atoms are given by

$$\sigma_{AB} = s\sigma \text{ and } \varepsilon_{AB} = e\varepsilon \quad (2)$$

where s and e are constants. In the particular case considered here, we have assumed that $s = 1.24$ and $e = 1.0$.

The potential is cut at the distance $r_{max} = 3.0\sigma$, and we do not use any long-range corrections.[50] Throughout this paper, the parameter ε is used as a unit of energy. Thus, we define the reduced temperature ($T^* = kT/\varepsilon$) and the reduced chemical potentials of both species ($\mu_i^* = \mu_i/\varepsilon$, $i = A, B$). All other energy-like quantities are also expressed in units of ε.

The mixture is then assumed to be placed in an external field of square symmetry, and the potential of that field is modeled using a simple cosine function

$$v(x, y) = V_b[\cos(2\pi x/a) + \cos(2\pi y/a)] \quad (3)$$

where V_b measures the corrugation of the potential and a determines its period. Here, we use a as a unit of length. In particular, we define $\sigma_{ij}^* = \sigma_{ij}/a$. Of course, V_b is expressed in units of ε as well. We also assume that the external field experienced by both components is the same.

The Hamiltonian of the model reads

$$E(\mathbf{R}_A, \mathbf{R}_B) = \sum_{i<j}^{N_A} u_{AA}(r_{ij}) + \sum_{i<j}^{N_B} u_{BB}(r_{ij}) + \sum_{i=1}^{N_A}\sum_{j=1}^{N_B} u_{AB}(r_{ij}) + \sum_{i=1}^{N_A} v(\mathbf{r}_i) + \sum_{i=1}^{N_B} v(\mathbf{r}_i) \quad (4)$$

In the above, $\mathbf{R}_A$ and $\mathbf{R}_B$ are multidimensional vectors representing the positions of all atoms of the components A and B in the system [$\mathbf{R}_i = (\mathbf{r}_{1_i}, \mathbf{r}_{2_i}, \ldots, \mathbf{r}_{N_i})$, i = A or B]. Throughout this work, we consider only the situation when the chemical potentials of both species are the same ($\mu_A^* = \mu_B^* = \mu^*$), so that the Hamiltonian (eq 4) can be written as

$$\mathcal{H}(\mathbf{R}_A, \mathbf{R}_B) = E(\mathbf{R}_A, \mathbf{R}_B) - \mu^* N \quad (5)$$

where $N = N_A + N_B$.

Although under the condition of $\mu_A^* = \mu_B^*$ one expects that on average the numbers of A and B particles are equal, computer simulations allow one to observe the formation of A-rich (or B-rich) phases due to finite size and metastability effects.

As already stated, we have chosen just one set of the parameters characterizing the mixture, while the corrugation of external potential has been varied.

The model has been studied using Monte Carlo simulation methods in the grand canonical and canonical ensembles.[51,52] Simulations have been carried out using square cells of the size $L \times L$, with L ranging between 20 and 48 and with standard periodic boundary conditions applied in both x and y directions. In the case of uniform systems (with $V_b = 0$), the simulation cell of arbitrary size can be used. In such cases, we have taken $L = 20$, 30, and 40. On the other hand, the study of systems subjected to an external potential requires careful analysis of the possible ordered states and the use of simulation cell sizes that properly take into account the periodicities of the ordered phases. The simulation cell size must be a multiple of the unit cell sizes for all ordered structures expected to appear in the system. Following the results of the ground state calculations discussed in part I, we have used $L = 24$, 36, and 48.

The recorded quantities included the average numbers of particles A and B, the average densities (per unit surface area) of the fluid−fluid, $\langle e_{gg}^* \rangle$, and the fluid−external field, $\langle e_{gs}^* \rangle$, energies, the total energy $\langle e^* \rangle$, the heat capacity, and the radial distribution functions, $g_{ij}(r)$, for ij = AA, AB, and BB.

III. Results and Discussion

A. Uniform System. Before we address the problem of the influence of the corrugation potential on the structure and phase behavior of symmetrical mixtures, we shall briefly discuss the properties of the uniform system (with the corrugation parameter V_b set to zero). The results for this system will serve as reference states.

In the considered case of $s = 1.24$ and $e = 1.0$, we have expected to observe the condensed phases (liquid and solid) of the structures similar to those found by Vlot and Van der Eerden,[46] who studied similar systems. These authors have observed the formation of mixed liquid and solid phases, both consisting of meandering thin stripe-like clusters of like particles, which they called spaghetti liquid and spaghetti solid. Our simulations have also demonstrated the formation of such phases. Figure 1 shows representative examples of snapshots obtained at $T^* = 0.4$ and at two different values of the chemical potential, in the regions corresponding to liquid (part a) and solid (part b) phases, respectively. One should note that the spaghetti solid is locally hexagonally ordered.

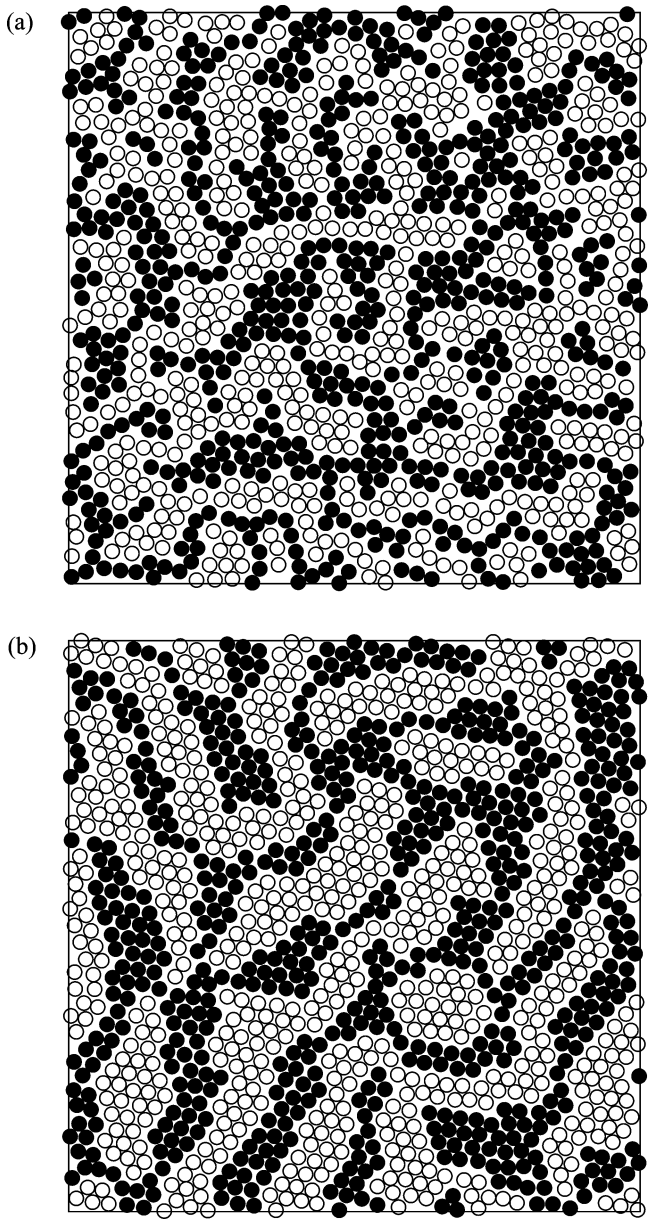

Figure 1. Examples of snapshots recorded for the uniform mixture at $T^* = 0.40$ and different values of the chemical potential $\mu^* = -0.60$ (part a) and -0.20 (part b).

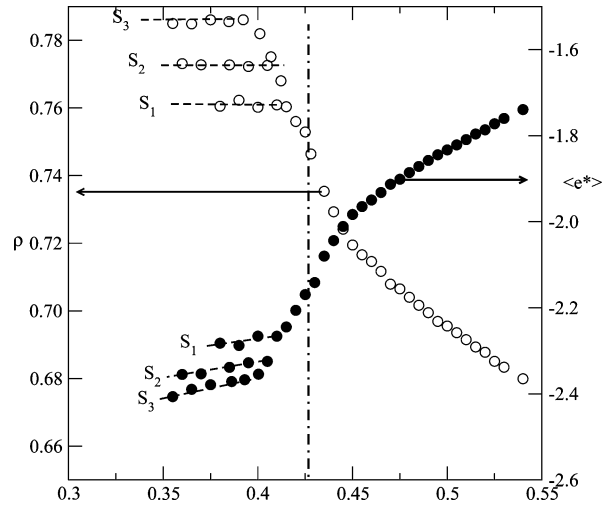

Figure 2. Changes of the total density and energy with temperature obtained for the uniform system at $\mu^* = 0.0$. Different solid-like states are labeled by S_1, S_2, and S_3. The vertical dash−dotted line marks the location of the heat capacity maximum.

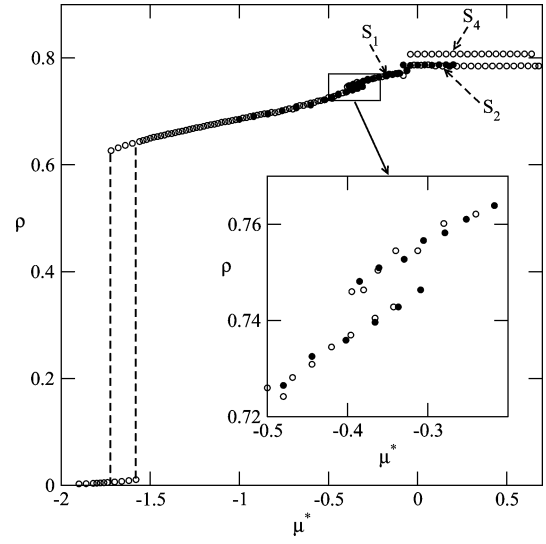

Figure 3. Isotherm of the uniform system, recorded at $T^* = 0.40$. Open and filled circles correspond to the results obtained for different sizes of the simulation cell, equal to $L = 20$ and 40, respectively. The inset shows the framed part in enlarged scale.

Figure 2 shows the temperature changes of the total density and energy obtained from three independent freezing runs, all carried out at the fixed value of the chemical potential, $\mu^* = 0.0$. At first sight, the results resemble the behavior of glass forming fluids[53,54] rather than the freezing of a liquid into a crystalline solid. Three different solid-like phases (marked as S_1, S_2, and S_3) have been found. The vertical dash−dotted line in Figure 2 marks the location of the heat capacity maximum.

Vlot and van der Eerden have suggested that the transition between the spaghetti liquid and spaghetti solid is of first order. Our data are quite consistent with that picture. In Figure 3, we present an example of an isotherm recorded at $T^* = 0.4$ and obtained from two independent runs. The isotherm shows the condensation of gas into spaghetti liquid as well as the formation of solid-like phases of different densities. One should note that two of them have the same densities as the states S_1 and S_2 (see Figure 2), while the third (labeled as S_4) has a density considerably higher than any of the states S_1, S_2, and S_3. The different solid-like structures that appear are most likely to be metastable states. Since the "observation time" in simulations is rather short and the energy barriers between different states are very large, the system remains trapped in a metastable state even when very long runs are performed.

In order to characterize the relaxation dynamics of the system, we have calculated the self-diffusion coefficient. In two dimensions, it is given by

$$D = \lim_{t\to\infty} \frac{\langle d^2(t)\rangle}{4t} \tag{6}$$

where

$$\langle d^2(t)\rangle = \frac{1}{N}\sum_{i=1}^{N} \langle |\mathbf{r}_i(t) - \mathbf{r}_i(0)|^2\rangle \tag{7}$$

is the mean square displacement after time t (measured in Monte Carlo steps) and N is the number of particles in the system. Our calculations have demonstrated that at a temperature of $T^* = 0.4$ the self-diffusion coefficient in spaghetti liquid is 4 orders

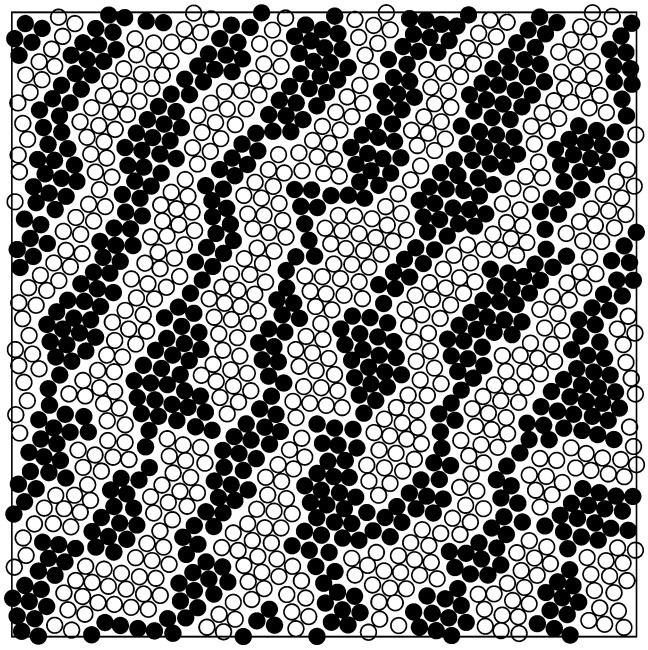

Figure 4. Configuration recorded for the uniform mixture at $T^* = 0.40$ and the chemical potential $\mu^* = -0.04$.

of magnitude higher than in the case of state S_1, which is equal to about 1×10^{-7}. Self-diffusion coefficients of other solid-like states (S_2, S_3, and S_4) are still lower than in state S_1, since the increasing density hinders the movement of atoms more strongly.

From the inspection of configurations corresponding to different solid-like phases, it follows that the structure changes from spaghetti-like (phase S_1, Figure 1b) to stripe-like (phase S_4, Figure 4).

Using the results obtained from Monte Carlo calulations, we have been able to construct the phase diagram for this system (see Figure 5). The points on the line marking the fluid−solid coexistence have been estimated using the locations of the heat capacity maxima and correspond to the formation of the solid-like S_1. We have not been able to obtain any reliable estimations of transition points between different solid-like phases. From our results, we conclude that the critical temperature of the gas−liquid transition is located at $T_c^* \approx 0.5$, and is only slightly lower than the critical temperature of one-component two-dimensional Lennard-Jones fluid, which is equal to 0.51 ± 0.02. On the other hand, the triple point temperature, $T_t^* \approx 0.305$, is considerably lower than in the case of one-component fluid, which is equal to $T_t^* = 0.40$.

Both effects are rather easy to explain. The potential energy of spaghetti liquid is only slightly lower than the potential energy of one-component liquid at the same density and temperature, since we have assumed that $e = 1$. On the other hand, the mixed liquid phase has higher entropy than one-component liquid. These two competing effects seem to compensate, and hence, the critical temperatures of the mixed spaghetti liquid and one-component liquid phases do not differ much. Of course, when the interaction between unlike particles is lowered ($s < 1$), then one also expects a lowering of the critical temperature of mixed liquid with respect to the one-component system. A rather large lowering of the triple point temperature with respect to the one-component system is due to large entropic effects, which destabilize the mixed solid phase.

B. Nonuniform Systems. Now we turn to the main part of our study and present the results for the systems subjected to the external potential of finite corrugation.

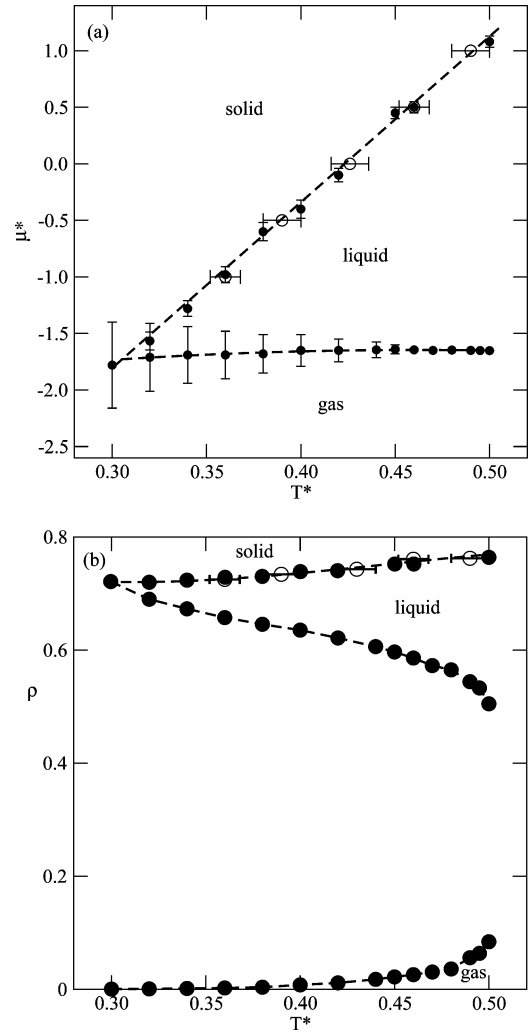

Figure 5. The μ^*-T^* (part a) and $\rho-T^*$ (part b) projections of the phase diagram for the uniform system. Filled circles are the results obtained from the isotherms, while open circles give the results obtained from series of Monte Carlo runs carried out at the fixed chemical potential and different temperatures.

With our choice of $\sigma^* = 1.0$ and $s = 1.24$, only pairs of like particles can occupy adjacent sites of the square lattice generated by the corrugation potential. A pair of unlike atoms can occupy next nearest sites being separated by the distance $r_{2NN}^* = \sqrt{2}$. It should be mentioned that similar one-component Lennard-Jones atoms with $\sigma/a = 1.24$ have been demonstrated to exhibit a stable commensurate $c(2 \times 2)$ structure.[55] Therefore, we can expect the existence of mixed commensurate phases with A−B nearest pairs separated by the distance $r_{2NN}^* = \sqrt{2}$. The parameter $e = 1.0$ has been chosen to avoid enhanced demixing (for $e < 1.0$) or mixing (for $e > 1.0$).

From the ground state considerations, presented in part I, it follows that such systems can order into different commensurate, high-order commensurate, as well as incommensurate mixed phases, depending on the magnitude of the potential barrier between adjacent sites, V_b, and the density. For future reference, we reproduce (see Figure 6) the ground state phase diagram for the system considered here. The ground state calculations did not involve incommensurate phases, likely to appear when the external potential corrugation is low enough, and hence, such phases have not been included in the phase diagram shown in Figure 6.

The central result of our study is a sort of phase diagram, which shows the chemical potentials (Figure 7a) and the

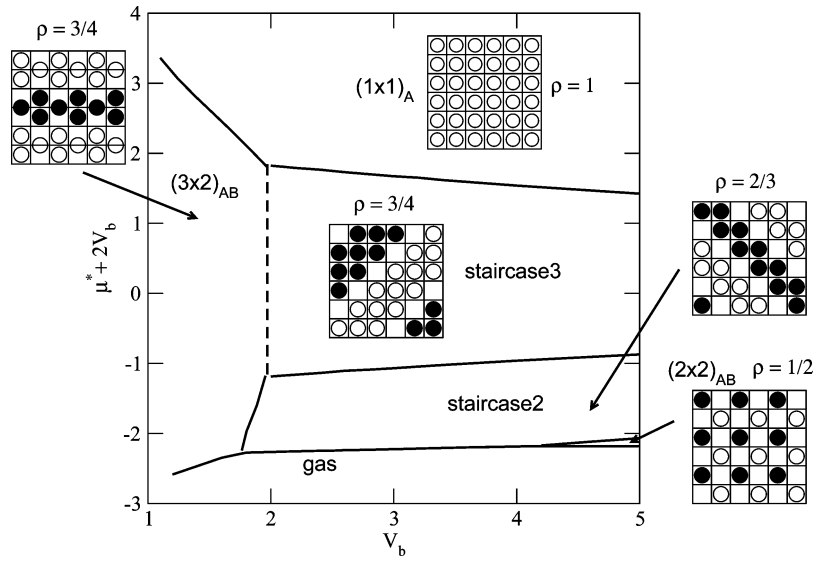

Figure 6. Changes of the ground state behavior with V_b for the system with $\sigma^* = 1.0$, $s = 1.24$, and $e = 1.0$. The insets show the structures and densities of different ordered phases.

densities (Figure 7b) at the coexistence between different phases as functions of the corrugation parameter V_b at the fixed temperature of $T^* = 0.4$. In general, we can state that the results are quite consistent with the ground state predictions.

Already for a very weakly corrugated external potential, with $V_b = 0.05$, we have found quite pronounced changes in the structure of a solid-like phase with respect to the uniform system. Instead of a spaghetti solid phase, in which the clusters of unlike particles are randomly oriented, we observe the formation of a striped axially ordered phase, as that shown in Figure 8a. Part b of Figure 8 demonstrates that within each stripe formed by like atoms the ordering characteristic for the high-order commensurate (3×2) structure appears. Of course, the ordering is not perfect and the thickness of stripes fluctuates along the simulation cell. The atoms are quite well axially ordered along the axis perpendicular to the stripes. On the other hand, the liquid phase has a disordered spaghetti structure quite the same as in the uniform system (see Figure 9). This picture remains qualitatively unchanged when the corrugation of the external potential increases up to $V_b \approx 1.6$. The only effect of increasing corrugation is the gradual increase of the solid-like phase stability leading to the increase of the triple point temperature at which the gas, liquid, and solid phases coexist. Of course, an increase of the corrugation leads to the gradual increase of localization of atoms over the lattice sites in the liquid phase. Nevertheless, the liquid retains the spaghetti structure.

From the results given in Figure 7, it follows that the triple point temperature increases above the temperature considered ($T^* = 0.40$) as soon as the corrugation parameter, V_b, exceeds the value of about 0.25. We have estimated triple points for different values of V_b between 0.1 and 1.6 and found nonmonotonous changes of T_t^* with V_b (see Figure 10). This result is quite consistent with the results shown in Figure 7 and can be explained by considering the influence of the external potential on the stability of the $(3 \times 2)_{AB}$ phase. When the corrugation is small, this phase becomes unstable at rather low temperatures. Low potential barriers for diffusion and the tendency for phase separation both cause the formation of domains consisting of like atoms, in which a distorted hexagonal ordering develops. When the corrugation increases, it stabilizes the atoms in registry positions and leads to an increase of the triple point temperature.

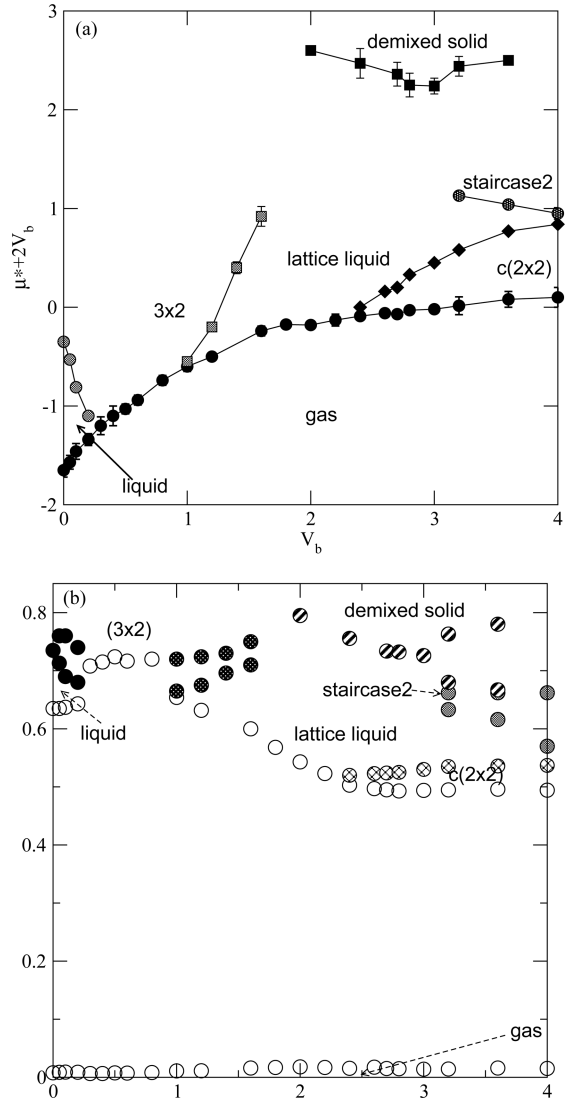

Figure 7. Chemical potential (part a) and densities (part b) at the coexistence between different phases versus the corrugation parameter for the system with $\sigma^* = 1.0$, $s = 1.24$, and $e = 1.0$ at the fixed temperature of $T^* = 0.40$.

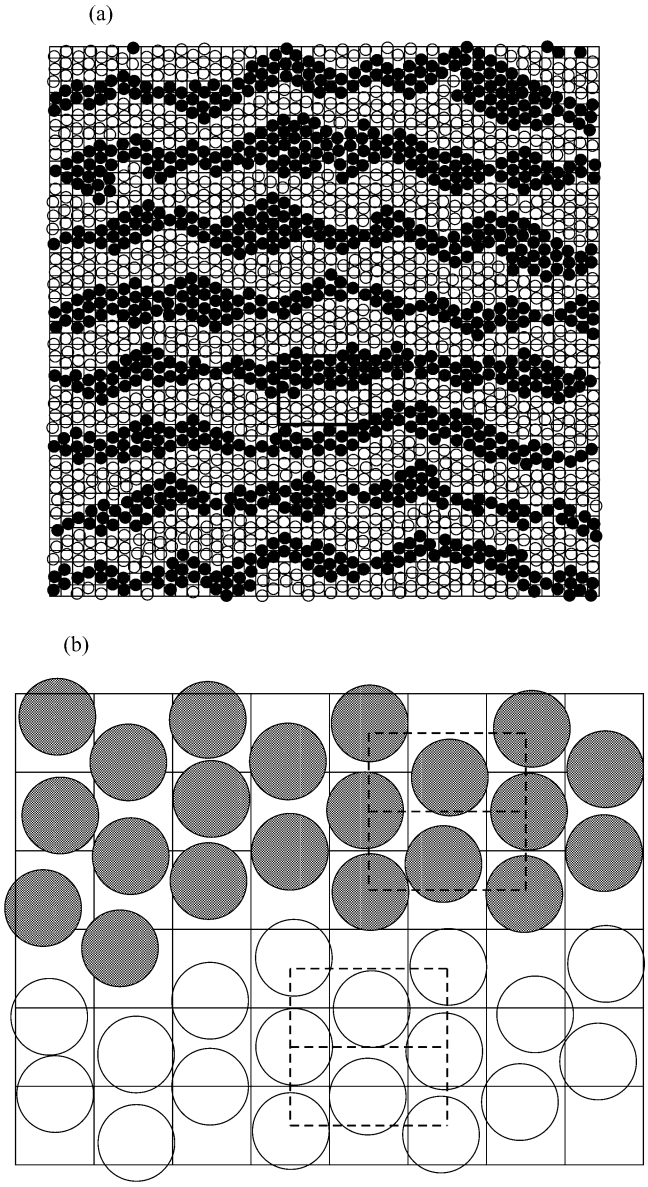

Figure 8. (part a) Snapshot for the system with $V_b = 0.05$ recorded at $T^* = 0.40$ and $\mu^* = -0.20$. (part b) The enlargement of the framed region of the snapshot.

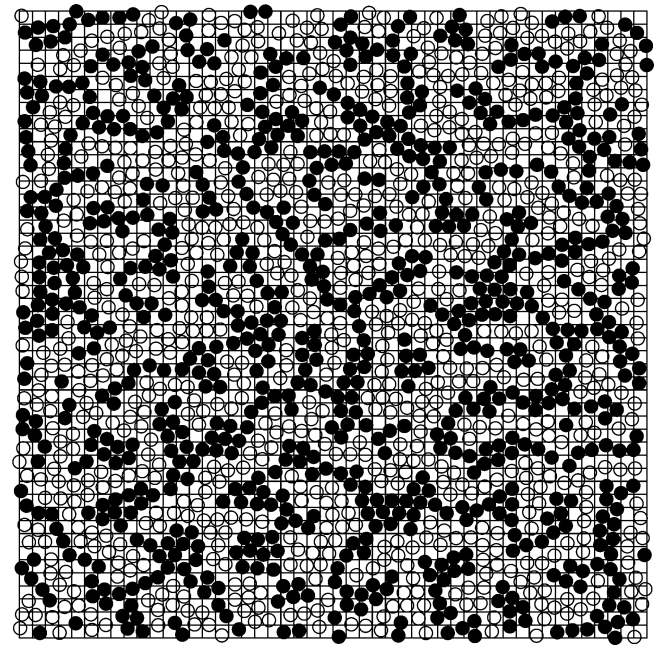

Figure 9. Snapshot demonstrating the spaghetti liquid for the system with $V_b = 0.05$ recorded at $T^* = 0.40$ and $\mu^* = -1.0$.

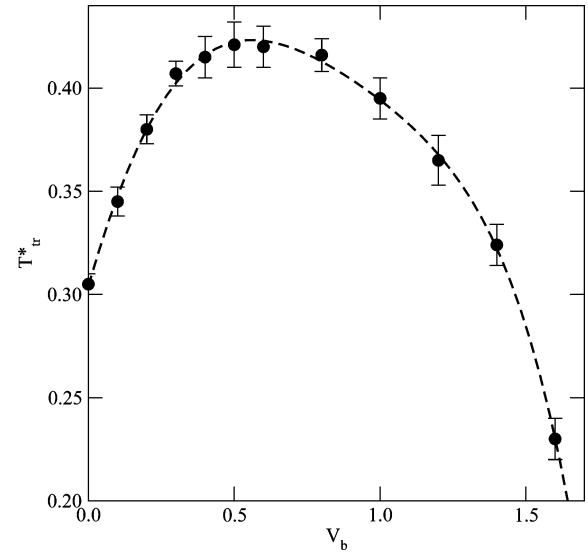

Figure 10. Triple point temperature plotted versus the corruption parameter.

When, however, the corrugation exceeds a certain threshold value, being close to $V_b \approx 0.6$, the atoms located over the saddle points are pushed toward the registry positions, and hence, the high-order commensurate $(3 \times 2)_{AB}$ phase is destabilized at the temperature decreasing with V_b.

As the chemical potential increases, the high commensurate $(3 \times 2)_{AB}$ phase transforms into a still denser striped phase, characterized by thicker stripes formed by like atoms. Figure 11 presents the isotherm recorded at $T^* = 0.4$ for the system with $V_b = 1.2$, and the insets show the examples of snapshots recorded in different regions. The isotherm exhibits four plateaus of different densities. The inspection of snapshots in different regions of the isotherm has shown that in all cases the system has the same stripe-like structure. Only the average thickness of the stripes changes. The density difference between the two subsequent structures is equal to about 0.021 and corresponds to $L/2$ A and $L/2$ B atoms (L being the linear dimension of the simulation cell). In all cases, the structure within stripes is the same and shows the ordering characteristic for the high-order commensurate $(3 \times 2)_{AB}$ structure, which in thick stripes forms a distorted hexagonal lattice. This is illustrated by the enlarged framed parts of the snapshots shown as insets to Figure 11. These enlargements also demonstrate that solid-like phases are quite well axially ordered. It is rather difficult to say, however, whether this series of structures corresponds to stable or to metastable states.

Ultimately, one expects a complete phase separation to occur and the formation of only two thick stripes: one consisting of A atoms and the other of B atoms. Extremely large metastability effects have excluded the possibility to estimate the location of such demixing transition. Nevertheless, we have observed the phase separation, leading to the formation of large clusters consisting of like particles as well as a complete phase separation, accompanied by the removal of one component from the system. Figure 12 shows the isotherm for the system characterized by $V_b = 1.8$, obtained at $T^* = 0.4$, and the examples of snapshots recorded at different values of the chemical potential. It is quite well seen that the isotherm does

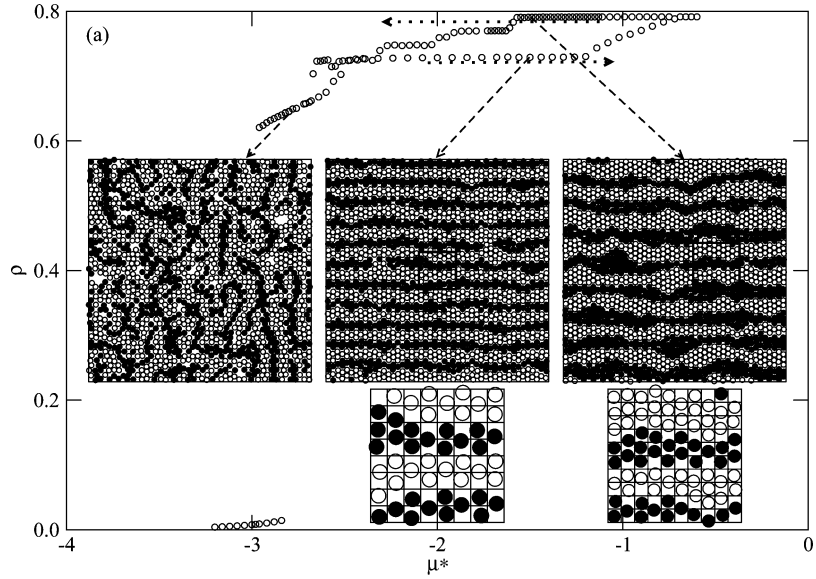

Figure 11. Isotherm at $T^* = 0.40$ obtained for the system with $V_b = 1.20$ and the size of the simulation cell equal to $L = 36$. The upper insets show typical configurations in different regions. The lower insets demonstrate the development of ordering characteristic for the (3×2) structure. Horizontal dotted lines mark the parts of the isotherm obtained for increasing and decreasing chemical potential.

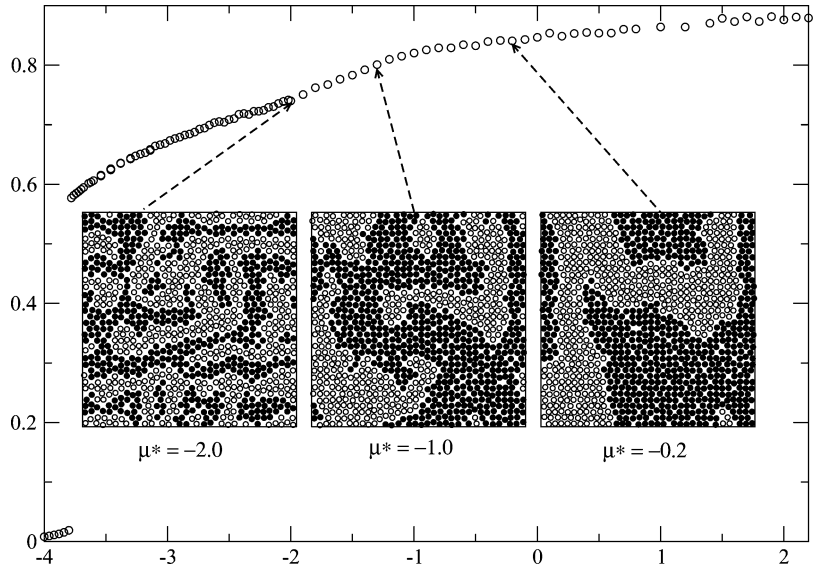

Figure 12. Isotherm at $T^* = 0.40$ obtained for the system with $V_b = 1.80$ and the size of the simulation cell equal to $L = 36$. The insets show typical configurations in different regions.

not exhibit the anomalies observed for lower values of V_b, while the structure of the condensed phase changes when the chemical potential changes. It should be noted that the isotherm given in Figure 12 involves the runs corresponding to the increasing and decreasing chemical potential and no trace of metastable states is observed.

The insets to Figure 12 domonstrate that what we observe here is a phenomenon very similar to spinodal decomposition. It should be emphasized, however, that even very long runs, consisting of 10^{11} Monte Carlo steps, performed at the fixed chemical potential and temperature, have not led to any appreciable changes of the structures presented in the insets to Figure 12. The formation of large clusters of like particles is most likely driven by the increase of density induced by the increasing chemical potential. In the case of usual spinodal decomposition, the size of clusters increases with time at the same density.

The formation of clusters of gradually increasing size along the isotherm also results from the corrugation potential. In the systems considered, a pair of like particles can occupy adjacent sites, while unlike particles can be located only on a pair of sites separated by a distance equal to $r^* = \sqrt{2}$, i.e., being the next nearest neighbors. The increasing chemical potential favors the formation of large clusters made of like atoms and leads to the gradual increase of the total density. Of course, such a clustering is enhanced when the corrugated surface potential becomes stronger. This explains why we have observed a complete phase separation, accompanied by the removal of one component in the systems with large values of V_b exceeding 3.0. It should be noted that such a phase separation has also been predicted by the ground state calculations (cf. Figure 6), which demonstrated that at sufficiently high chemical potentials the stable state corresponds to the (1×1) phase consisting of one component only.

It should be noted that for V_b exceeding 1.6 we have not observed the formation of the stripes and the ordering characteristic for the $(3 \times 2)_{AB}$ structure at all. In order to monitor the formation of axially ordered striped structures, we have

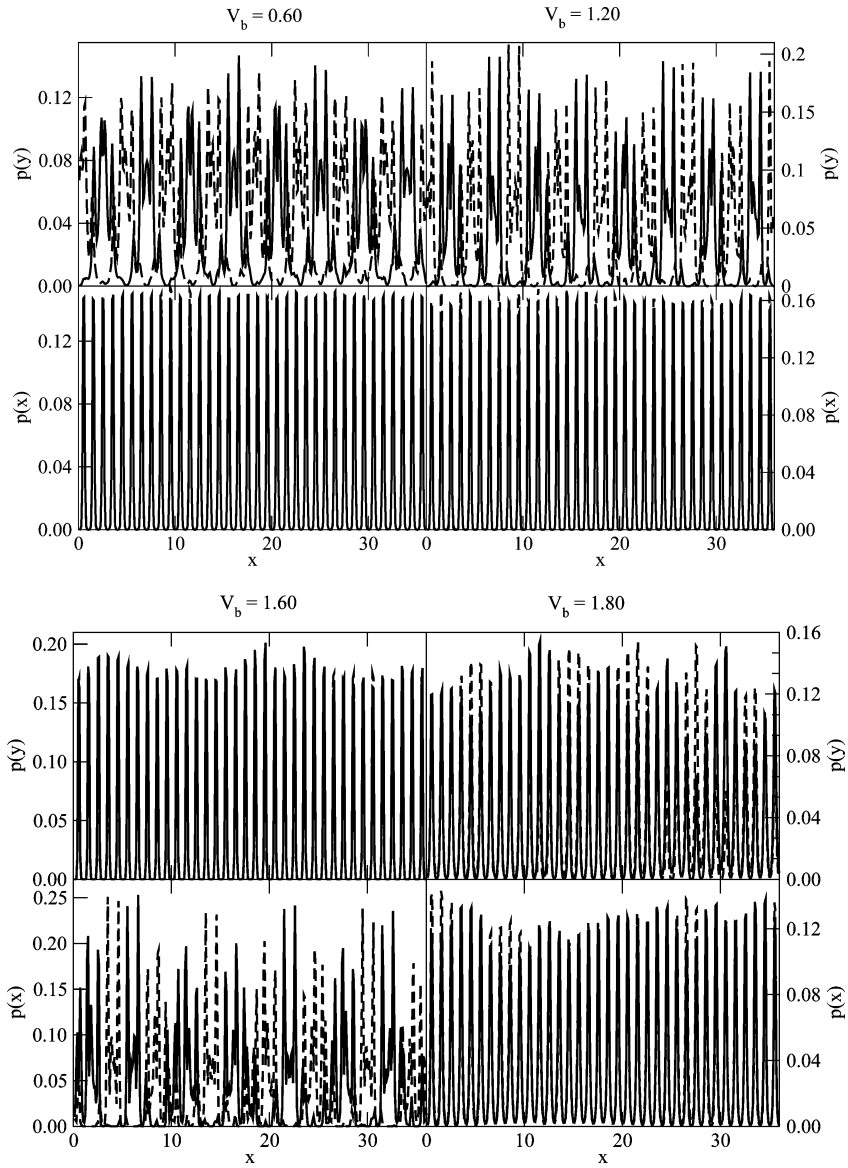

Figure 13. Density distributions along the x (lower panels) and y (upper panels) axes calculated at $T^* = 0.40$ and $|mu^* = -1.50$ for the systems characterized by different values of the corrugation parameter V_b (shown in the figure). Solid and dashed lines mark the distributions for different species.

calculated the distributions of atom densities along the two symmetry axes (x and y) for different values of the corrugation parameter and the results are given in Figure 13. It is quite evident that for $V_b \leq 1.6$ the systems exhibit axial ordering along one axis and the formation of stripes along the second symmetry axis. On the other hand, for $V_b = 1.8$, the distributions do not show any trace of the striped structure and the distributions along both axes demonstrate that atoms are quite well localized over the external potential wells. Of course, we expect that upon lowering the temperature the upper limit of the corrugation parameter allowing for the development of stripes along one of the system symmetry axes should move toward higher values. Note that the ground state calculations predict that the ordering characteristic for the $(3 \times 2)_{AB}$ structure should be stable up to $V_b \approx 1.95$. At finite temperatures, thermal excitations cause atoms to not be likely to sit over the saddle points as predicted for the $(3 \times 2)_{AB}$ structure. Figure 13 demonstrates that already for $V_b = 0.60$ the atoms are displaced from the saddle points at the temperature considered.

For the corrugation parameter $V_b \geq 2.4$, the formation of the mixed commensurate $c(2 \times 2)$ phase over a certain range of chemical potentials has been found. This phase appears to be disordered with respect to the arrangement of A and B atoms over the lattice. One should note that the ground state calculations predict the formation of a perfect $(2 \times 2)_{AB}$ ordered structure, being the $c(2 \times 2)$ commensurate phase in which the atoms A and B occupy different sublattices, for V_b exceeding about 4.11 (cf. Figure 6). In our previous work, we have demonstrated that the ordered $(2 \times 2)_{AB}$ phase transforms into the disordered $c(2 \times 2)$ phase at very low temperatures, much lower than the temperature considered here. Of course, the stability region of the commensurate $c(2 \times 2)$ structure depends on both the magnitude of V_b and on the temperature. At a fixed temperature of $T^* = 0.4$, we observe the gradual increase of the chemical potential region over which the commensurate phase retains stability. This is illustrated by the results shown in Figure 14, depicting a series of isotherms as well as the order

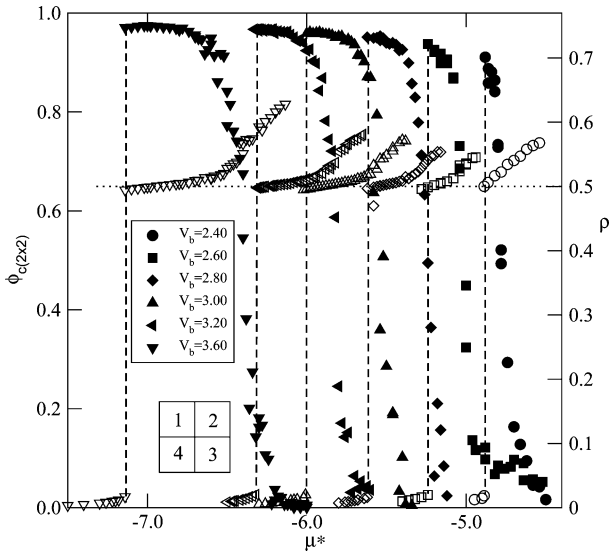

Figure 14. Isotherms (at $T^* = 0.40$) and the isothermal changes of the order parameter $\phi_{c(2\times2)}$ (see eq 9) for the systems characterized by different values of V_b (shown in the figure). The inset shows how the square lattice has been divided into four sublattices.

parameter suitable to detect the $c(2 \times 2)$ structure. This order parameter is defined as

$$\phi_{c(2\times2)} = |\rho_{A,1} + \rho_{B,1} + \rho_{A,3} + \rho_{B,3} - \rho_{A,2} + \rho_{B,2} - \rho_{A,4} - \rho_{B,4}| \quad (8)$$

where $\rho_{K,i}$ ($i = 1, 2, 3, 4$) and $K =$ A or B is the density of species K on the ith sublattice. The division of a square lattice into four sublattices is shown in the inset to Figure 14. Upon the increase of the chemical potential, the density gradually increases, leading to the occupation of the sublattices which are not occupied in the commensurate phase. Figure 14 displays only those parts of the isotherms recorded during Monte Carlo runs which involve the condensation of gas into the commensurate phase and the disordering of the commensurate phase. From the ground state calculations, it follows (cf. Figure 6) that for the corrugation parameter $V_b \in [1.75, 4.11]$ the gas condensation leads to the formation of the ordered structure, called "*staircase*2 ", of density $\rho = 2/3$. Our Monte Carlo calculations at $T^* = 0.40$ have shown that this phase is stable only for $V_b \geq 3.2$. It appears, however, that the *staircase*2 phase becomes stable at lower values of V_b when the temperature is lowered. Figure 15 shows a series of isotherms obtained for the system with $V_b = 2.8$ and demonstrates that at temperatures up to $T^* = 0.36$ there are quite wide regions of the chemical potential over which the *staircase*2 phase is stable. This figure also shows the behavior of the order parameter suitable to detect phase separation, defined as

$$|m| = \frac{|\rho_A - \rho_B|}{\rho_A + \rho_B} \quad (9)$$

and calculated at the temperatures equal to $T^* = 0.36$ and 0.40. Large metastability effects made it impossible to obtain reliable results at lower temperatures. The results presented suggest that the phase separation is a continuous transition, but we cannot rule out the possibility of a discontinuous (first-order) transition. In fact, we have found a discontinuous phase separation for larger values of $V_b = 3.2$ and 3.6.

The insets to Figure 15 show the snapshots obtained at $T^* = 0.40$ (lower inset) and $T^* = 0.34$ (upper inset) both recorded at a density equal to about 2/3. It is evident that at $T^* = 0.34$ a

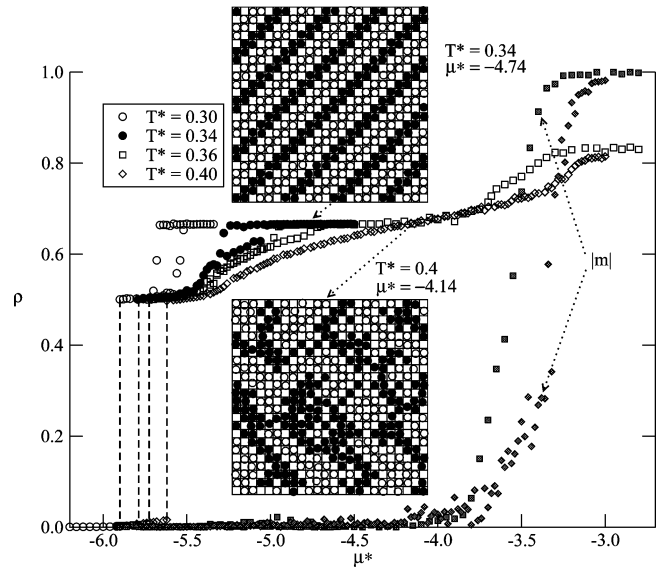

Figure 15. Isotherms and the order parameter $|m|$, defined by eq 9, for the system characterized by $V_b = 2.8$ at different temperatures. Note that the order parameter is shown only for the isotherms recorded at $T^* = 0.36$ (shaded squares) and 0.40 (shaded diamonds). The insets show the snapshots recorded at different temperatures and at the density corresponding to the ordered phase *staircase*2.

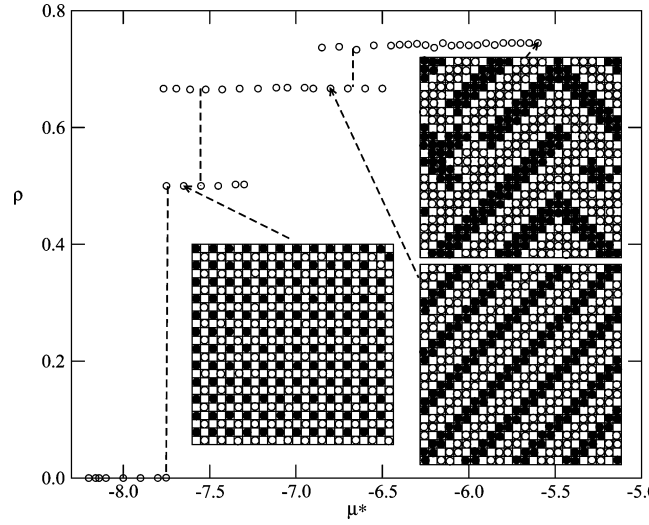

Figure 16. Isotherm at $T^* = 0.22$ obtained for the system with $V_b = 3.60$ and the size of the simulation cell equal to $L = 24$. The insets show the configurations corresponding to different ordered phases.

perfectly ordered *staircase*2 phase is formed, while at $T^* = 0.40$ only small domains of the ordering characteristic of the *staircase*2 phase are present.

The results shown in Figure 15 do not show any trace of the *staircase*3 phase, predicted by the ground state calculations (cf. Figure 6) to appear in between the *staircase*2 and the $(1 \times 1)_A$ structures. In fact, one expects a series of striped structures characterized by different stripe width to be stable in the ground state. At finite temperatures, we have expected rather to observe stripes of fluctuating width. Nevertheless, the formation of the *staircase*3 phase has been found at sufficiently low temperatures. Figure 16 presents the isotherm recorded at $T^* = 0.22$ for the system characterized by $V_b = 3.6$ and showing the presence of well developed ordered $c(2 \times 2)_{AB}$ and *staircase*2 phases as well as the *staircase*3 phase. The insets show the examples of configurations corresponding to the different condensed phases. For this particular choice of V_b, the commensurate $c(2 \times 2)_{AB}$

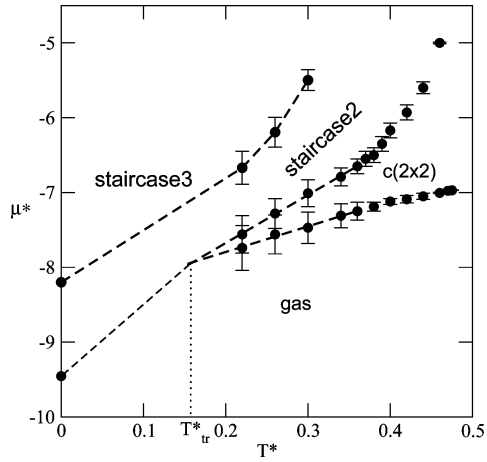

Figure 17. μ^*-T^* projection of the phase diagram for the system characterized by $V_b = 3.6$.

phase is not expected to be stable in the ground state. Although we have not been able to construct the low temperature part of the phase diagram due to extremely large metastability effects, our results suggest (see Figure 17) the existence of the triple point (in which the gas, $c(2 \times 2)_{AB}$, and *staircase*2 phases coexist) at a temperature of about 0.15.

Although we have not attempted to estimate the location of the order−disorder transition of the $c(2 \times 2)_{AB}$ structure, the isotherms recorded at different temperatures have shown that at temperatures exceeding $T^* = 0.30$ the distribution of atoms A and B between sublattices is more or less uniform, while at $T^* = 0.26$ a nearly perfect $c(2 \times 2)_{AB}$ structure is still present.

IV. Final Remarks

We are aware that our results lack generality, since only one set of the parameters describing the system geometry ($\sigma^*_{AA} = 1.0$ and $s = 1.24$) has been considered. Also, the parameters representing the strength of interaction between AA, BB, and AB pairs have been assumed to be the same. Nevertheless, the results have confirmed the predictions of ground state calculations.

The uniform system, with the corrugation potential switched off, is found to form a series of solids of different densities. All of them exhibit a local hexagonal order and consist of elongated clusters made of like particles. The low density solid-like phases show the spaghetti structure. The high density solid-like phases have been found to possess a stripe-like structure.

It has been shown that even a weakly corrugated external potential of square symmetry transforms the spaghetti-like solid phases into axially ordered mixed solid-like phases. At low corrugations of the external potential, the stripes made of like atoms exhibit the ordering characteristic of the high-order $(3 \times 2)_{AB}$ commensurate phase. The thickness of stripes has been observed to increase with the increasing chemical potential, leading to a sort of staircase of phase transitions. Ultimately, this process leads to phase separation. Of course, the appearance of the ordering corresponding to the high-order $(3 \times 2)_{AB}$ commensurate phase is a consequence of our choice of the model parameters, and primarily by the assumed values of $\sigma^* = 1.0$ and $s = 1.24$. The increase of the external field corrugation above $V_b = 1.6$ causes the $(3 \times 2)_{AB}$ ordering to become unstable at the temperature considered ($T^* = 0.40$). It should be noted that the ground state calculations have shown that the limit of stability of the striped $(3 \times 2)_{AB}$ phase occurs at still higher corrugation, corresponding to $V_b \approx 1.95$.

A highly corrugated external field leads to the appearance of different mixed epitaxial structures, in agreement with the ground state considerations. In particular, the formation of ordered and disordered $c(2 \times 2)$ structures as well as striped structures of different stripe widths has been confirmed.

In future work, we shall discuss the systems characterized by different values of σ^*_{AA}, s, and e.

Acknowledgment. The authors would like to acknowledge stimulating discussions with Dr. Kurt Binder (University of Mainz, Germany).

This work was supported by Polish Ministry of Science under Grant No. N N202 046137.

References and Notes

(1) Monson, P. A.; Steele, W. A.; Henderson, D. *J. Chem. Phys.* **1981**, *74*, 6431.
(2) Barker, J. A.; Henderson, D.; Abraham, F. F. *Physica A* **1981**, *106*, 226.
(3) Klain, J. R.; Cole, M. W. *Faraday Discuss. Chem. Soc.* **1985**, *80*, 71.
(4) Cuadros, F.; Mulero, A. *Chem. Phys.* **1993**, *177*, 53.
(5) Abraham, F. F. *Phys. Rep.* **1981**, *80*, 339.
(6) Phillips, J. M.; Bruch, L. W.; Murphy, R. D. *J. Chem. Phys.* **1981**, *75*, 5097.
(7) Tabochnik, J.; Chester, G. V. *Phys. Rev. B* **1982**, *25*, 6778.
(8) Udink, C.; Frenkel, D. *Phys. Rev. B* **1987**, *35*, 279.
(9) Rovere, M.; Nielaba, P.; Binder, K. *Z. Phys. B* **1993**, *90*, 215.
(10) Rovere, M.; Heermann, D. W.; Binder, K. *J. Phys.: Condens Matter* **1990**, *2*, 7009.
(11) Dash, J. G. *Contemp. Phys.* **2007**, *43*, 427.
(12) Kosterlitz, M.; Thouless, P. J. *J. Phys. C* **1973**, *6*, 1181.
(13) Halperin, B. I.; Nelson, R. D. *Phys. Rev. Lett.* **1978**, *41*, 121.
(14) Nelson, R. D.; Halperin, B. I. *Phys. Rev. B* **1979**, *19*, 2457.
(15) Young, A. P. *J. Phys. C* **1978**, *11*, L453.
(16) Young, A. P. *Phys. Rev. B* **1979**, *19*, 1855.
(17) Dash, J. G. *Films on Solid Surfaces*; Academic Press: New York, 1975.
(18) *Ordering in Two Dimensions*; Sinha, S. K., Ed.; North-Holland: Amsterdam, The Netherlands, 1980.
(19) *Phase Transitions in Surface Films*; Dash, J. G., Ruvalds, R., Eds.; Plenum Press: New York, 1980.
(20) Venables, J. A. *Introduction to Surface and Thin Film Processes*; Cambridge University Press: Cambridge, U.K., 2000.
(21) Binder, K. In *Cohesion and Structure of Surfaces*; de Boer, F. R., Pettifor, D. G., Eds.; Elsevier: Amsterdam, The Netherlands, 1995.
(22) Bruch, L. W.; Cole, M. W.; Zaremba, E. *Physical Adsorption: Forces and Phenomena*; Clarendon Press: Oxford, U.K., 1997.
(23) Patrykiejew, A.; Sokolowski, S.; Binder, K. *Surf. Sci. Rep.* **2000**, *37*, 207.
(24) van Konynenburg, P. H.; Scott, R. L. *Philos. Trans. R. Soc. London, Ser. A* **1980**, *298*, 48.
(25) Rowlinson, J. S. Swinton, F. L. *Liquids and Liquid Mixtures*, 3rd ed.; Butterworths: London, 1982.
(26) Panagiotopoulos, A. Z.; Quirke, N.; Stapleton, M.; Tildesley, D. J. *Mol. Phys.* **1988**, *63*, 527.
(27) de Miquel, E.; del Rio, E. M.; Telo da Gama, M. M. *J. Chem. Phys.* **1995**, *103*, 6188.
(28) Wilding, N. B. *Phys. Rev. Lett.* **1997**, *78*, 1488.
(29) Wilding, N. B. *Phys. Rev. E* **1997**, *55*, 6624.
(30) Wilding, N. B.; Schmid, F.; Nielaba, P. *Phys. Rev. E* **1998**, *58*, 2201.
(31) Kahl, G.; Schöll-Paschinger, E.; Lang, A. *Monatsh. Chem.* **2001**, *132*, 1413.
(32) Schöll-Paschinger, E.; Levasque, D.; Weis, J.-J.; Kahl, G. *Phys. Rev. E* **2001**, *64*, 011502.
(33) Antoneych, O.; Forstmann, F.; Diaz-Herrera, E. *Phys. Rev. E* **2002**, *65*, 061504.
(34) Wilding, N. B. *Phys. Rev. E* **2003**, *67*, 052503.
(35) Pini, D.; Tau, M.; Parola, A.; Reatto, L. *Phys. Rev. E* **2003**, *67*, 046116.
(36) Schöll-Paschinger, E.; Gutlederer, E.; Kahl, G. *J. Mol. Liq.* **2004**, *112*, 5.
(37) Woywod, D.; Schoen, M. *Phys. Rev. E* **2006**, *73*, 011201.
(38) Köfinger, J.; Wilding, N. B.; Kahl, G. *J. Chem. Phys.* **2006**, *125*, 234503.
(39) Jacques, J., Collet, A. Wilen, S. H. *Enantiomers, Racematers and Resolutions*; Krieger: Malabar, FL, 1991.

(40) Vlot, M. J.; Claasen, S.; Huitema, H. E. A.; van der Eerden, J. P. *Mol. Phys.* **1997**, *91*, 19.
(41) Patrykiejew, A.; Sokolowski, S.; Pizio, O. *J. Phys. Chem. B* **2005**, *109*, 14227.
(42) Gunton, J. D.; San Miquel, M.; Sahni, P. In *Phase Transitions and Critical Phenomena*; Domb, C., Lebowitz, J. L., Eds.; Academic Press: New York, 1983; Vol. 8.
(43) Mauri, R.; Shinnar, R.; Triantafyllou, G. *Phys. Rev. E* **1998**, *58*, 7691.
(44) Leptoukh, G.; Strickland, B.; Roland, C. *Phys. Rev. Lett.* **1995**, *74*, 3636.
(45) Binder, K., Fratzl, P. In *Phase Transformations in Materials*; Kostorz, G., Ed.; Wiley: Weinheim, Germany, 2001.
(46) Vlot, M. J.; van der Eerden, J. P. *J. Chem. Phys.* **1998**, *109*, 6043.
(47) Assoud, L.; Messina, R.; Löwen, H. *J. Chem. Phys.* **2008**, *129*, 164511.
(48) Sengupta, S.; Marx, D.; Nielaba, P.; Binder, K. *Phys. Rev. E* **1994**, *49*, 1468.
(49) Sałamacha, L.; Patrykiejew, A.; Sokołowski, S. *J. Phys. Chem. B* **2009**, *113*, 13687–13696.
(50) Frenkel, D.; Smit, B. *Understanding Molecular Simulation: From Algorithms to Applications*; Academic Press: San Diego, CA, 1996.
(51) Allen, M. P.; Tildesley, D. J. *Computer Simulation of Liquids*; Oxford University Press: Oxford, U.K., 1987.
(52) Landau, D. P.; Binder, K. *A Guide to Monte Carlo Simulation in Statistical Physics*; Cambridge University Press: Cambridge, U.K., 2000.
(53) Zallen, R. *The Physics of Amorphous Solids*; Wiley: New York, 1983.
(54) Debenedetti, P. G.; Stikkinger, F. H. *Nature* **2001**, *410*, 259.
(55) Patrykiejew, A.; Sokolowski, S. *J. Phys. Chem. C* **2007**, *111*, 15664.

JP908710E